PROCEEDINGS, 49th Workshop on Geothermal Reservoir Engineering
Stanford University, Stanford, California, February 12-14, 2024
SGP-TR-227

Using Borehole Failure Geometry and Stress Measurements to Study Stress-Strength Profiles in Geothermal Projects

Farid Zabihian[1], Asmae Dahrabou[1], Reza Sohrabi[1], Andrés Alcolea[2], Peter Meier[2], Benoît Valley[1]

[1] Centre for Hydrogeology and Geothermics (CHYN), University of Neuchâtel, Neuchâtel, Switzerland

[2] Geo-Energie Suisse AG, Zürich, Switzerland

farid.zabihian@unine.ch

Keywords: Deep geothermal projects, stress profiles, borehole breakout, drilling-induced tensile fractures, borehole failure, stress tensor

ABSTRACT

One of the key elements of reservoir characterization in deep geothermal projects is the determination of the in-situ stress state. A good knowledge of the stress state allows designing well drilling operation for borehole stability. The stress state is also a key control in deep seated fluid flow geological brittle structures and to assess the potential response of such structures to stimulation and production operations. Comprehensive assessment of in-situ stress, rock strength, and ongoing evaluation of wellbore failure, such as breakouts (BOs) and Drilling-Induced Tensile Fractures (DITFs), is vital. Analyzing failure data, especially from tools like acoustic televiewer logs, provides valuable insights into rock strength, in-situ stress, and their interactions near the borehole.

We present here the results from a workflow initially proposed by Dahrabou et al. (2022) for interpreting borehole failure data using analytical and empirical solutions. We are currently working at improving the method to increase its applicability to various deep geothermal project. The method allows for producing profiles with depth that includes heterogeneous distributions of stress tensor components, directions, cohesion, and friction. Such results enhance our understanding of stress and strength variabilities within the earth crust and are useful for developing sustainable geothermal reservoirs. The results of this study reveal plausible sets of stress and strength parameters that closely replicate the complex breakout distribution observed in the studied boreholes and reservoirs. Additionally, it sets the base for quantitative predictions of wellbore failure and risk analyses. These are essential for designing and implementing advanced borehole completions that facilitate zonal isolation, a crucial step in realizing the full potential of geothermal projects.

1. INTRODUCTION

Success of Enhanced Geothermal System (EGS) relies on various factors including drilling performance which is a critical consideration throughout the entire process of deep geothermal projects, encompassing both the drilling and operational phases. One effective strategy to ensure borehole stability, thereby averting costly drilling delays, involves deviating the well in alignment with the most advantageous orientation relative to the in-situ stress conditions. However, this trajectory often differs from the one that intersects a sufficient number of pre-existing fractures, which are the primary targets for stimulation. Moreover, the fractures that are intersected may not be conducive to hydro-shearing stimulation. In addition, a non-uniform borehole cross-section, characterized by deep borehole breakouts (BOs) or drilling-induced tensile fractures (DITFs), can complicate or prevent the proper placement of packers as means of well completion in further development of projects. Sealing with packers is essential for the targeted stimulation of pre-existing fractures.

To mitigate the aforementioned risks, it is crucial to conduct a comprehensive assessment of the in-situ stress conditions and rock strength, as well as evaluate wellbore failure before and especially during the drilling process (Zang and Stephansson, 2010). Most stress measurement techniques provide punctual and local measurements and are not well suited to provide a full stress characterization including its variability. Borehole breakouts if they occur is one of the only methods allowing to characterize some component of the stress state along a borehole and thus to assess stress variability. Methods to assess stress from borehole failure are common in the literature (Zoback et al., 2003, Zoback, 2007). Here we propose to use such methods to generate stress profile with depth including stress variability. We use for this a two-step process that consist first in estimating linear (depth dependent) trend (first order approximation). At this step we include a common assumption that one principal stress is considered to be vertical and its magnitude, Sv, is estimated as the weight of the overburden. Since density variations are typically small in most rocks the integration of the overburden weight generate profile that are close to linearity. In a second step we focus on the characterization of stress variation. We aim to capture the perturbations around the trend which arise from any sources of rock heterogeneity such as the presence of faults, fractures or any other source (second order approximation).

In the first-order approximation, the magnitudes of horizontal stress can be estimated using depth linear trends (Zoback et al., 2003). Such methods are widely applied in geothermal projects such as Häring et al., (2008), Valley and Evans, (2019), Mastin et al., (1991), Borm et al., (1997). Such methods are sensitive to their initial assumptions for example different failure criteria leads to different estimates of S_{Hmax} magnitude, in cases that the effect of the intermediate principal stress, σ_2, is considered or not. Hydraulic tests like XLOTs (Lin et al, 2008) are employed to assess the minimum horizontal principal stress, denoted as S_{hmin}. The direction of BOs often serves as a reliable indicator of the orientation of S_{hmin}. As proposed by Zoback et al., (2003) the geometry of BOs along the borehole allows for the inference of a linear trend of S_{Hmax}. Furthermore, the challenge of estimating rock strength properties, which are crucial for the subjectively chosen

failure criterion, is compounded by the difficulty in obtaining accurate data from available boreholes. An alternative method involves estimating these properties through empirical relationships between strength and petrophysical parameters, derived from sonic and density logs (Chang et al, 2006). While these relationships can be refined with laboratory measurements on cores, the constraints are evident due to the time-consuming, expensive, and often non-representative nature of laboratory tests, which are typically conducted at a single depth.

Current methods for estimating stresses and strength properties often rely on uncertain strength estimates, creating a significant unreliability on their outputs. This study addresses this gap by enhancing the workflow which was initially developed by Dahrabou et al. (2022) as a systematic methodology to simultaneously estimate depth profiles of local stress tensor characteristics (including magnitudes and orientations of all three principal stresses) and rock strength properties (cohesion and friction). We present here this methodology recalling the key elements form Dahrabou et al. (2022) paper and we illustrate the methodology using data from the deep geothermal borehole BS-1 in Basel, Switzerland. We discuss limitations of the methodology and on-going improvement of the workflow.

2. METHODOLOGY

Both trends (first-order approximation) and variations around the trend (second-order) can be estimated for each unknown. Model parameters are derived using the regularized pilot points method (Alcolea et al., 2006), implemented in PEST (Parameter ESTimation, Doherty, 2003), based on borehole cross-sectional characteristics and the presence/absence of DITFs (Axial and En-echelon Drilling Induced Tensile Fractures). The Kirsch analytical solution (Kirsch, 1898) is utilized to estimate the stress state around the borehole, considering all stress components, including thermal stresses from borehole wall cooling. Furthermore, this methodology suggested here is carried out in an iterative manner and at each borehole cross-section. The main steps of the algorithm are described in detail in Dahrabou et al. (2022) paper, but in the following, they are briefly described:

Step 1: inputting a set of initial parameters that we call "starting points" (such as depth trends of magnitudes, stress orientation, wellbore orientation, Poisson's ratio, thermo-elastic parameters, etc.) and utilizing the Kirsch analytical solution to compute stresses around the borehole.

Step 2: assessing failure conditions, with the Mohr–Coulomb and Mogi–Coulomb criteria currently implemented; however, any other failure criterion can be integrated without loss of generality.

Step 3: the evaluation includes breakout width, extent, orientation, and the presence of DITFs.

Step 4: an objective function (a penalty function) is assessed to measure the deviation of the solution from available measurements, encompassing geometric features, prior estimates, or direct parameter measurements.

Step 5: encompasses modifying parameters and returning to Step 1 iteratively until achieving the minimum of the objective function, constituting the parameter estimation, optimization, or broadly, the inverse problem (Carrera et al., 2005). This workflow is executed using the PEST generic parameter estimation software.

2.1 Calculation of the near-field state of stress

Determining the near-field state of stress involves analytically or numerically calculating the stress redistribution caused by drilling and thermal effects. Analytical solutions are favored over complex numerical borehole models due to their well-established standard practice in borehole design, computational efficiency, and ease of implementation. The methodology outlined here focuses on achieving fast and reliable calculations allowing for systematic parameter estimation scanning a large portion of possible solutions. Efficient calculation is also needed in practice for on-site decision-making limiting downtime in the drilling process. For this study, we employ an elastic analytical solution (Schmitt et al., 2012), specifically the Kirsch closed-form solution, to compute stress redistribution around the borehole. Our implementation considers scenarios where the borehole is not aligned with one of the principal stresses, incorporating a thermo-elastic stress component to simulate residual stresses from borehole wall cooling during drilling. The stress distribution is computed in two main steps. Initially, the stress tensor is expressed in a local and orthonormal borehole Cartesian coordinate system (u, v, w). Subsequently, Kirsch equations are solved to compute stress redistribution around the borehole in a cylindrical coordinate system with its origin at the center of the borehole.

2.2 Estimation of failure components (BOs and DITFs)

Borehole failure including BOs and DITFs, can be studied through interpretation of data from tools like acoustic televiewer logs. The analysis of failure observations, namely BOs and DITFs, offers valuable understanding of the strength of rock, the in-situ stress conditions, and their interactions in the immediate vicinity of the borehole. This approach, distinct from predominantly point-based methods like mini-frac tests, allows for the assessment of stress and strength along continuous 1D profiles which makes it possible to characterize statistically their variability along boreholes over relatively short distances. In this study, it is crucial to emphasize that the proposed method estimates model parameters based on measurements available during or shortly after drilling, such as breakout width, breakout extent/depth of penetration, breakout orientation (azimuth), and drilling-induced tensile fractures. These parameters are illustrated in figure 1.

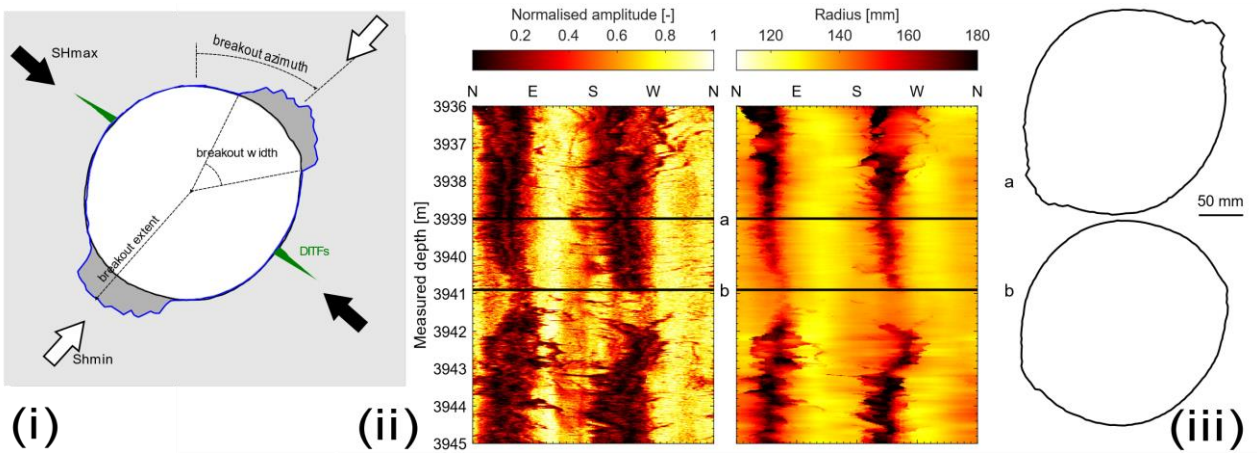

Figure 1: (i) Geometry of typical borehole breakouts and drilling induced tensile fractures, (ii) image-logs of an interval along borehole BS-1 in Basel (Switzerland); (iii) interpreted cross-sections of the borehole, showing the small scale heterogeneity of breakout geometry over short distances.

2.2.1 breakout width

The computation of breakout width, w_{BO}, involves assessing the failure criteria at the borehole wall (i.e., $r = a, \forall\ \theta$) using stresses calculated by the Kirsch closed-form solution. In this study Mohr–Coulomb criterion is used because it is the most used in practice, although Mogi–Coulomb criterion is also included in the workflow. The arc, measured as an angle, along which the failure criterion is satisfied provides an estimate of w_{BO}. The underlying assumption in this computation is that failure occurs at the cylindrical borehole wall, initially spanning a maximum width, with subsequent progressive extension (deepening) but without widening. Therefore, there is no need to simulate the gradual failure leading to the final breakout geometry. While some studies (i.e. Azzola et al., 2019) report modifications of breakout width with time in-situ, our methodology adopts a widely accepted approach.

2.2.2 breakout extent

Methods for computing breakout extent, e_{BO}, are limited in the existing literature. This scarcity is, in part, attributed to the prevalent use of breakout width for estimating the stress state. Breakout extent results from gradual failure progressively releasing stresses and extending failure deeper until reaching a stable section (Cuss et al., 2003). Simulating such processes is challenging, leading to the neglect of breakout extent as a by-product. Nevertheless, we contend that characterizing breakout extent is crucial for effective well completion, ensuring proper packer sealing, for instance. In the subsequent discussion, we explore computationally feasible alternatives for this characterization. Unfortunately, applying the same general principle as breakout width computation, i.e., evaluating the failure criteria for $r \geq a$ using the Kirsch solution, is not meaningful due to the neglect of progressive failure. Shen (2008) introduces an alternative empirical methodology, relying on numerical simulations of borehole failure through the FRACOD (Shen and Stephansson, 1994) fracture mechanics code. Shen's approach assumes a vertical borehole under plain strain conditions (as FRACOD is a 2-dimensional code), meaning one principal stress aligns with the borehole axis. Furthermore, it considers dry conditions—no pore pressure or internal borehole pressure. Shen derived relationships between stress conditions, strength parameters, and breakout extent based on these assumptions.

$$\frac{3\sigma_{Hmax} - \sigma_{hmin}}{C_o} = 1 + A\left(\frac{e_{BO}}{a} - 1\right)^B \tag{1}$$

where the term on the left represents the ratio of the maximum effective tangent stress to the uniaxial compressive strength. Within the constraints of Shen's relationship, the Kirsch solution simplifies, and the maximum effective hoop stress is given by $\sigma_{\theta\theta}^{max} = 3\sigma_{Hmax} - \sigma_{hmin}$, where σ_{Hmax} and σ_{hmin} represent the maximum and minimum effective principal horizontal stresses, respectively. The parameters A and B are regression parameters within a specified range (Shen, 2008). In spite of its non-linearity, Shen's approach is computationally affordable.

2.2.3 DITFs occurrence

The evaluation of drilling-induced tensile fractures follows the Rankine criterion:

$$\sigma_3 \leq T_0 \tag{2}$$

Here, T_0 represents the tensile strength (with negative values indicating tension). The calculation of the minimum effective principal stress at the borehole wall, σ_3, involves using the Kirsch solution. This computation incorporates the wellbore internal pressure and the thermal stress resulting from the cooling of the borehole wall. It is important to note that our implementation jointly considers both axial and en-echelon tensile fractures, referred to as A-DITFs and E-DITFs (Brudy and Zoback, 1993).

2.3 Parameter estimation

Typically, addressing parameter uncertainties involves parametric sensitivity analysis or manual trial-and-error calibration. In contrast, we approach the estimation problem using the mathematical framework of automatic inverse modeling. This approach liberates modelers from the complexities, tedium, and error-prone nature of manually testing various parameter combinations. In essence, inverse modeling involves extracting information about the model based on measurements of the modeled phenomenon (Carrera et al., 2005). Once a conceptual model is established, the inverse problem—also referred to as history matching, tomography, or calibration—entails determining the set (or sets) of parameters that best align with observations through the mapping equations mentioned above. This is achieved by minimizing a penalty function F, so-called objective function, which measures the misfit between calculated and observed values, arranged in vectors O and O^*, respectively, with components $O^*_i = \{\boldsymbol{w}^*_{\boldsymbol{BO}}, \boldsymbol{e}^*_{\boldsymbol{BO}}, \boldsymbol{\theta}^*_{\boldsymbol{b}}, \boldsymbol{D}^*\}$. The set of calibrated parameters, described below, is arranged in vector $\boldsymbol{M}$.

The objective function F can be expressed in a generic manner as:

$$F = \sum_{i=1}^{4} \lambda_i (\mathcal{O}_i - \mathcal{O}^*_i)^t \boldsymbol{V_i}^{-1} (\mathcal{O}_i - \mathcal{O}^*_i) + \sum_{j=1}^{npar} \beta_j (\mathcal{M}_j - \mathcal{M}^*_j)^t \boldsymbol{V_j}^{-1} (\mathcal{M}_j - \mathcal{M}^*_j) \quad (3)$$

where subscripts i and j stand for type of measurement ($i = 1$ for $\boldsymbol{w}^*_{\boldsymbol{BO}}$, $i = 2$ for $\boldsymbol{e}^*_{\boldsymbol{BO}}$, etc.) and parameter, up to $npar$ ($j = 1$ for parameters characterizing S_{Hmax}, $j = 2$ for those of S_{hmin}, etc.). The scalars λi and βj are global calibration weights that balance the contribution of the individual pieces of information. Matrices Vi and Vj are the corresponding prior covariance matrices, containing information about the initial uncertainty of each measurement/parameter type and the possible cross-correlations between them.

The parameterization of the problem is contingent on the intended characterization. For a first-order characterization targeting depth trends, parameters are represented in a generic manner as follows:

$$p = a \cdot \mathrm{TVD} + b \quad (4)$$

2^{nd} order characterization aims at estimating the deviations of a given parameter from its estimated mean (1^{st} order characterization), which enables the analysis of variability at all scales. To that end, we used the regularized pilot points method (Alcolea et al., 2006), originally devised by De Marsily, (1984), as implemented in the free parameter estimation software PEST. The generic parameterization now becomes:

$$p = a \cdot \mathrm{TVD} + b + \varepsilon\,(\mathrm{MD}) \quad (5)$$

where ε is the perturbation of a parameters around its trend and it depends on measured depth to account for deviated boreholes. Note that the parameter a multiplies TVD instead, because most geomechanical parameters are expressed as vertical depth gradients (e.g., principal stresses, (Häring et al. 2008)).

3. BS-1 DATA DESCRIPTION

In 2006, a 5 km deep borehole, named BS-1, was drilled in Basel, Switzerland, as part of a planned Enhanced Geothermal System (EGS) doublet. The wellbore, with a diameter of 9–7/8'' down to 4850 m MD, was then drilled further to 5009.4 m MD with a diameter of 8–1/2''. It is sub-vertical with a maximum deviation of 8°. The crystalline basement was characterized on-site through cuttings, with a 10 m core retrieved at 4909 m MD. The granitic basement rock composition is generally homogeneous, with variations in quartz content. Brittle shear zones and alterations are locally present (Kaser et al., 2007).

Fracture frequency decreases with depth, averaging 3.1, 1.3, and 0.3 fractures/m in depth ranges 2.6–2.65 km, 2.65–3.0 km (Ziegler et al., 2015), and below 3.0 km, respectively. The upper 400 m of the crystalline section is influenced by paleo-exhumation during the Permo-Carboniferous, potentially affected by pre-sedimentation exhumation or recent tectonic loadings. Ultrasonic borehole televiewer logs were obtained with azimuthal resolution between 2578 and 5001 m MD. Fluid velocity measurements were used to compute wellbore geometry. Extensive logging was conducted before setting a 7–5/8'' casing at 4638 m MD. A reservoir characterization was performed below the casing, followed by hydraulic stimulation in December 2006, resulting in a 3.4 magnitude event and project abandonment (Deichmann and Giardini, 2009).

3.1 BS-1 failure data

The borehole data used in our analysis and the procedure to infer borehole failure are described in Valley and Evans, (2009 and 2019). But it is also briefly described in the following. Breakouts were identified along 81% of the logged section and are almost continuous except for a large gap from 2747 m TVD to 2899 m TVD and some other minor gaps in scattered in the sections that high intensity of natural fractures is observed. Borehole geometry was averaged from the study of breakouts at cross sections with a 0.4 m longitudinal spacing. Breakouts are pervasive along BS-1 (81%), while only in 20% of the borehole DITFS are present.

No clear depth trends are apparent in the distribution of DITFs. This implies that throughout the entire borehole length, $\sigma_3^{\min}$ at the wellbore wall is close to tensile failure, and the additional hoop stresses resulting from the cooling of the borehole wall are adequate to locally induce tensile failure. Moreover, observations of DITFs are converted into the minimum hoop stress. When DITFs are present, the minimum hoop stress must be lower than the tensile strength ($To = -4$ MPa, where tension is negative), while the minimum hoop stress remains higher than the tensile strength in the absence of DITFs. To elaborate further, considering that 20% of the BS-1 profile is impacted by DITFs. We create a minimum hoop stress distribution that aligns with the observed occurrences of DITFs. This transformation allows us to convert the boolean DITFs observations (presence or absence) into a continuous variable, which is more suitable for our calibration algorithm.

As already observed by Valley and Evans (2019), breakout width, w_{BO} decreases with depth from an average of 94◦ in the 2.58–3 km section to 65◦ in the 4.5–5 km section. Normalized failure extension, e_{BO}/a, remains relatively constant with depth (only a slight increase with depth is observed). In addition, by considering all data, the average of θ_b is 54°.

4. SOLUTION NON-UNIQUENESS

The inverse problem is often plagued by issues of instability, non-identifiability, and non-uniqueness, as extensively discussed by Carrera and Neuman, (1986), demonstrates their close interrelation. Instability arises when minor changes in observations result in significant alterations in estimated parameters, addressed through model identification criteria (Medina and Carrera, 2003). Non-identifiability occurs when more than one set of parameters leads to a given solution of the forward problem. Non-uniqueness is observed when multiple parameter sets lead to a minimum of the objective function F. The results, reveal combinations of Co and S_{Hmax} that precisely reproduce the breakout geometry. Notably, for any given Co, there exists a S_{Hmax} value that exactly reproduces the observations, and the calibrated pairs of Co and S_{Hmax} exhibit almost linear correlation. This aligns with Barton's equation (1988), designed for estimating S_{Hmax} based on BOs width observations. However, Co is typically unknown, making the problem under-determined.

5. CALIBRATION OF THE DEVELOPED GEOMECHANICAL MODEL ON OBSERVED

The calibration results using measurements from 3 to 5 km MD are presented in this section. Initially, we concentrate on the first-order characterization, which involves estimating linear trends of parameters with depth. While we assert that first-order characterization is necessary, it alone is insufficient to ensure proper completion, such as cementing or packer sealing. Therefore, we delve into the variability of model parameters by calibrating the deviations from the trend at 201 pilot points, shared across all parameters (totaling 1407 pilot points). We refer to this as the second-order calibration stage.

5.1. First order calibration approach

To replicate BS-1 observations using our failure models, we concentrate on the model parameters that exert the most influence and cannot be estimated through other means. In this first-order calibration, we utilize a simplified profile with the depth of these model parameters. In summary, our stress/strength model is characterized by 9 parameters (namingly, slop and intercept of both *S1* and *S2*, a of Euler angels, friction, cohesion, Ashen and Bshen). To ensure the Levenberg–Marquardt algorithm converges to a global optimum, we employ multiple starting points in the calibration. For this purpose, the prior distribution of each parameter is randomly sampled, assuming a uniform distribution. This results in a total of 200 initial parameterizations exploring the global parameter space. However, initial rejection criterion, based on frictional equilibrium, is also applied to the initial starting points before choosing them. Initial sets of parameters that do not satisfy the specified constraints are discarded, and new sets are generated until the desired count of initial coherent parameterizations is reached. It is important to note that different initial parameter sets may result in distinct final optimum sets of calibrated parameters with a similar final value of the objective function F. This phenomenon is a well-recognized challenge in inverse problem theory, referred to as non-uniqueness.

5.1.1 Non-uniqueness of BS1 study

A posterior rejection criterion was defined by setting a maximum threshold for the objective function after calibration, and calibrated models with final objective function above the threshold were rejected. After this rejection process, 136 well calibrated models were kept using the Mohr–Coulomb to be studied for the step of second order. Figure 2 displays failure observations (w^*_{BO}, e^*_{BO}/a, θ^*_b, and D^*) alongside the 136 well-calibrated horizontal principal stresses, using the Mohr–Coulomb failure criterion. Notably, breakout width tends to decrease with depth, while breakout extent remains relatively consistent, aligning with the observations in the BS-1 borehole depicted in Fig. 2. This behavior can be attributed to the low slopes of calibrated stresses (aS_{Hmax} and aS_{hmin}, with mean values of 4.3 and 7.2 MPa/km, respectively; resembling experimental findings in Valley and Evans (2019). All models converge toward a breakout orientation $\theta^b = 54°$, precisely matching the orientation of S_{hmin} reported in Valley and Evans (2007).

The calibrated parameter range is generally extensive, emphasizing the non-uniqueness of the inverse problem discussed in previously. This non-uniqueness underscores the inherent uncertainties in parameters and can be mitigated by incorporating either additional measurements of a specific type or diverse types of measurements. In the context of this study, the influence of the number of measurements was assessed by omitting certain cross-sections.

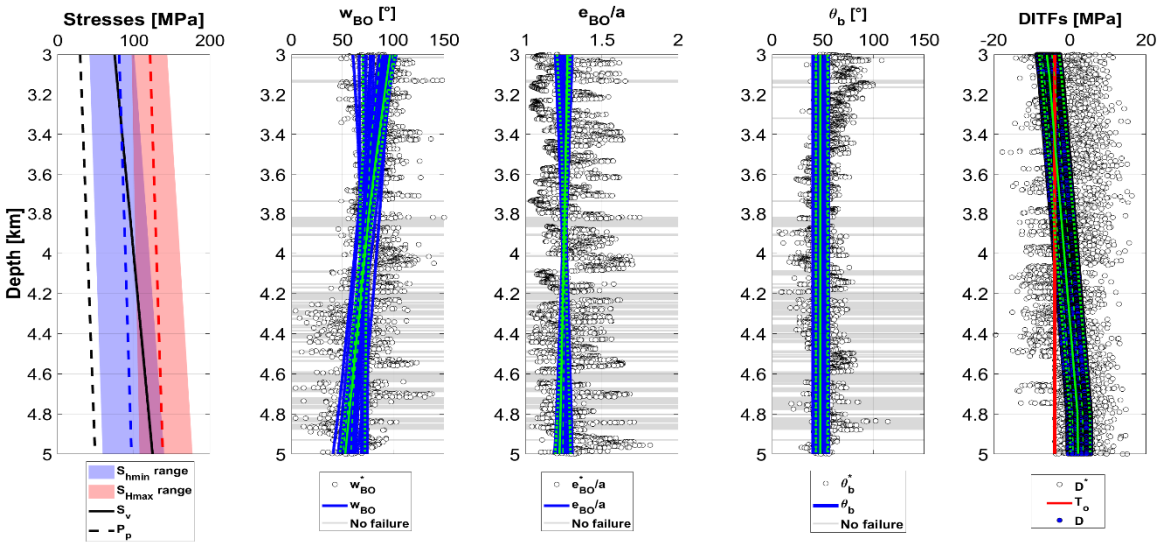

Figure 2: 1st order calibration results utilizing the Mohr–Coulomb failure criterion. From left panel to right, (1) The range of calibrated $SHmax$ (pink) and $Shmin$ (purple) for 136 different starting points, with Sv and pore pressure profiles represented by solid and dashed black lines, respectively. The blue and red dashed lines depict the mean of the calibrated ranges for $Shmin$ and $SHmax$, respectively; (2) calibrated and measured breakout width; (3) normalized breakout extent; (4) breakout orientation; (5) DITFs.

5.2. Second order calibration approach

The initial calibration at the 1st order, provides practical insights into the overall trends of stress and strength along the borehole, portraying mean conditions. However, it does not capture the local variations crucial for completion scheme design, especially in natural systems like rock masses where such variations can be substantial. Quantifying this variability is essential for designing completion schemes, including packers, as these local conditions can be more severe than average conditions, leading to completion problems. To address this, a 2nd order calibration is undertaken, using 1st order parameter values leading to the median profile of $SHmax$ in Fig. 2. For brevity, only one calibration is presented, utilizing the Mohr–Coulomb failure criterion. Each parameter intervening in model equations is now parameterized with pilot points regularly spaced every 10 m. The pilot point discretization is uniform across all strength and stress parameter profiles, resulting in an overall parameterization involving 1407 pilot points. Ordinary kriging is employed as the spatial interpolation algorithm to generate continuous profiles from values at pilot points.

The results, including goodness of fit and derived parameters, are presented in Figs. 3 and 4, respectively. The 2nd order calibrated outputs (Fig. 3) not only capture the observed trends but also the corresponding small-scale variabilities. The goodness of fit is notable, with root mean square errors of 10°, 0.086, 9°, and 4.6 MPa for breakout width, normalized extent, orientation, and DITFs, respectively. The initial misfits from the 1st order calibration was higher (27°, 0.175, 25°, and 11.5 MPa). The 2nd order calibrated outputs successfully reproduce most of the gaps without breakouts (shaded blue areas in Fig. 3a) and most of the maxima/minima of normalized extent (Fig. 3b). While extreme values along measured profiles are not precisely captured due to limitations in pilot points and potential undesired oscillations, the derived parameters in Fig. 4 exhibit coherence and plausibility. The stress profiles of $SHmax$ and $Shmin$ align well with the reported transitional regime at ≈4800 m depth. Strength parameter profiles (panels b to d) show values consistent with the literature. The interplay between stress and strength is appropriately captured by the 2nd order model, indicating a general negative correlation between stress and strength peaks at gaps in the absence of breakouts. Breakout orientation exhibits minimal departures (± 5°) from the median value of 144°, as reported in Häring et al. (2008). Lastly, Shen's parameters defining the failure model fall within standard limits (Shen, 2008).

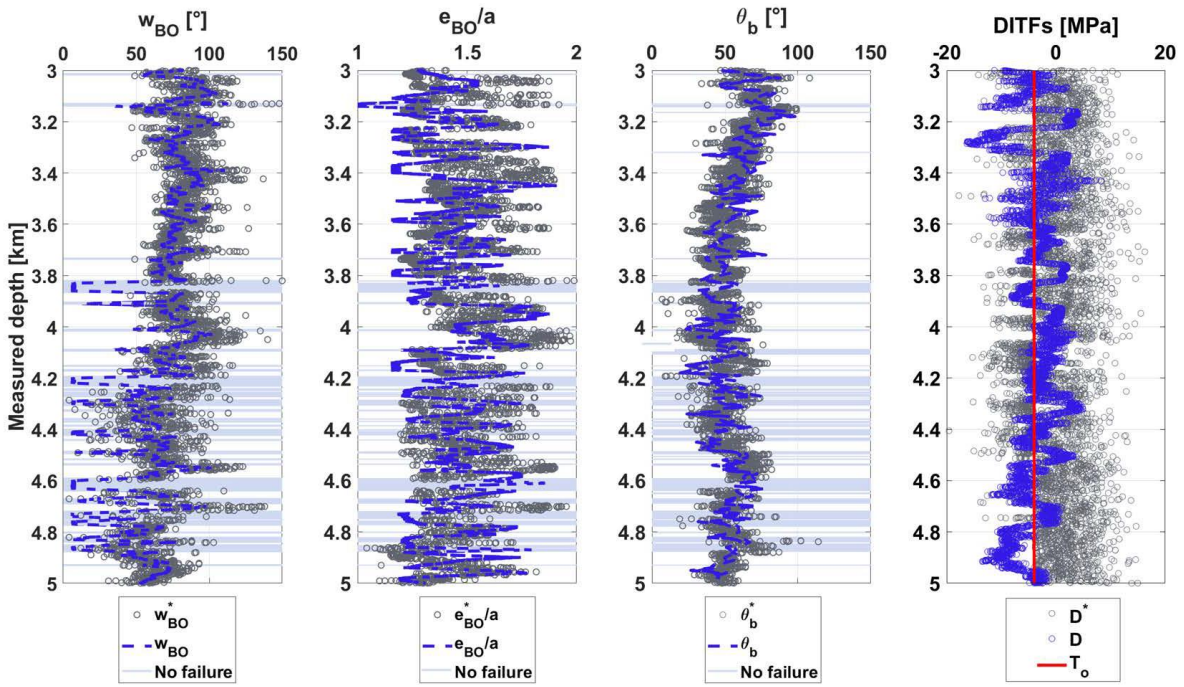

Figure 3: Calibrated failure profiles using pilot points method from 3 to 5 km. from left to right: (1) breakout width; (2) breakout extent; (3) breakout orientation; (4) Transformed and calibrated DITFs. In (1) – (3), the grey circles correspond to failure observations while in (4) they depict the estimated minimum hoop stress derived from DITFs observations. In (1) – (4), the dashed blue lines correspond to the calibrated failure using Mohr–Coulomb criterion. Light blue shaded areas in panels (1), (2) and (3) correspond to depths with no breakouts. The red line in panel (4) shows the tensile strength, $To = -4$ MPa.

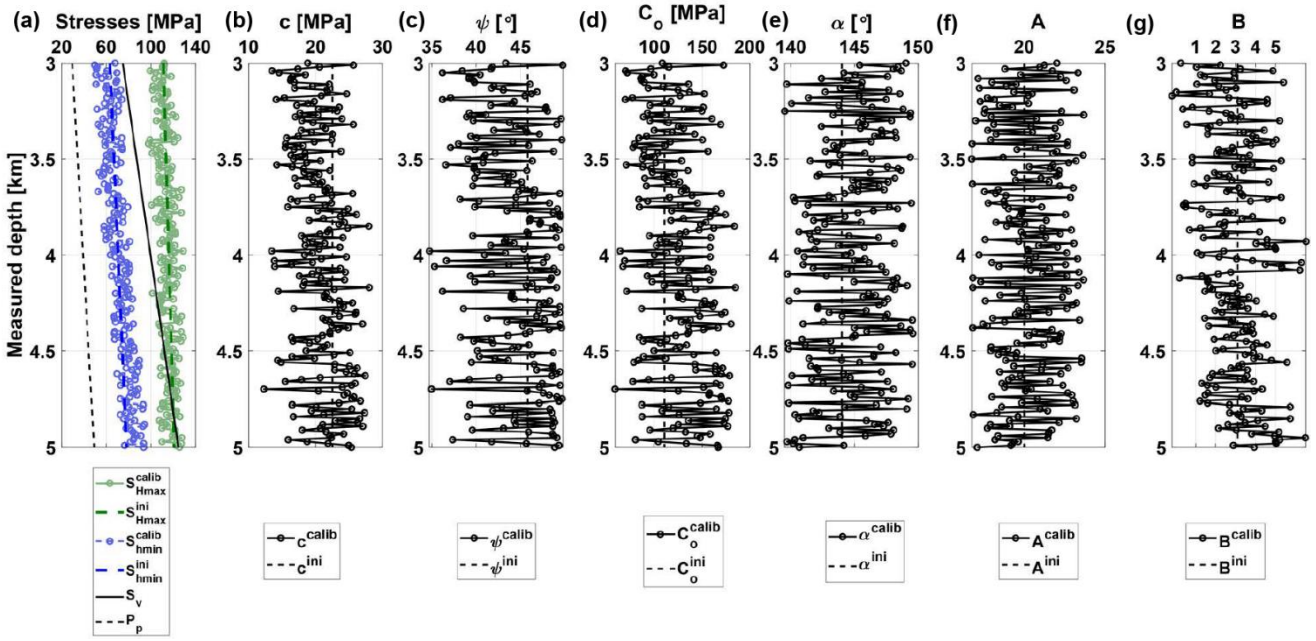

Figure 4: Calibrated input parameters profiles using pilot points method from 3 to 5 km. from left to right: (1) minimum and maximum principal horizontal stresses $SHmax$ and $Shmin$; (2) Cohesion; (3) internal friction angle; (4) uniaxial compressive strength; (5) the angle α of Euler and finally the regression parameters of Shen (6) A and (7) B. The dashed lines in all panels correspond to the initial depth profiles.

6. DISCUSSION

6.1. Failure models evaluation

Our assessment of failure models enables us to scrutinize the reliability of failure criteria in replicating borehole failure observations. Theoretically, models incorporating the strengthening effect of the intermediate principal stress, such as the Mogi–Coulomb criterion, are expected to more comprehensively capture failure processes compared to models neglecting this effect (e.g., the Mohr–Coulomb criterion). The profiles obtained using the Mohr–Coulomb criterion, align with the observed stress regime, acknowledging the transitional regime at approximately 4800 m MD. These findings are consistent with the observations of Valley and Evans (2019).

In evaluating the failure criterion, it is essential to note that we employed the Kirsch closed-form solution for stress computation due to its computational efficiency and ease of implementation. However, this analytical solution has limitations as it does not account for progressive failure and assumes constant initial breakout width post-initiation of failure, potentially resulting in underestimation of borehole failure parameters. On the other hand, the Mohr–Coulomb failure criterion may overestimate failure parameters by neglecting the strengthening effect of the intermediate stress. Despite these considerations, we find the Mohr–Coulomb criterion suitable for our application as it balances conservative and non-conservative effects, yielding stress and strength estimates consistent with independent stress observations.

6.2. Stresses trends with depth

Our initial 1^{st} order model calibration offers insights into the depth trends of stress magnitudes, aligning with observations by Valley and Evans (2019). However, this probabilistic model calibration broadens the range of possible solutions, enhancing confidence in stress characterization. A notable feature in the calibrated profiles of $SHmax$ and $Shmin$ is their low gradient with depth, explaining the observed decrease in breakout width in BS-1. Regularization, information constraints, and incorporating $Shmin$ data from other sources such as hydraulic stimulation assists in reducing solution uncertainty. The geodynamic explanation for the observed low stress gradient, especially in $Shmin$, remains uncertain and may be influenced by factors like cooling profiles and stiffness contrast. Examining breakout width in fractured zones reveals continuous gaps, particularly in areas with intense natural fractures. A 1^{st} order calibration in specific zones indicates lower stress magnitudes and isotropic stress conditions in the fractured zone, possibly influenced by a perturbed stress state due to pre-sedimentation exhumation or recent tectonic loading.

6.3. Limitations and applicability of the methodology

The described methodology, proven highly effective on BS-1, is mathematically generic and applicable to various case studies. Despite its success, there are inherent limitations. Notably, the inclusion of breakout extent, a crucial parameter for zonal isolation, poses challenges due to the difficulty in its computation. While empirical methods, as employed, offer solutions, further enhancements using complex mathematical approaches, like the semi-analytical method proposed by Setiawan and Zimmerman (2020), are possible.

Addressing the absence of borehole BOs is another challenge. BOs' absence hinders insights into the stress–strength state, impacting the calibration process. In cases with limited BO occurrences, ill-posed inverse problems may arise. Adding a penalty criterion to the objective function, accounting for the presence/absence of breakouts, could help. Similarly, evaluating DITFs requires careful consideration, and a similar criterion for presence/absence of breakouts can be applied.

While the BS-1 borehole is mostly sub-vertical, applying the methodology to deviated boreholes should not pose additional difficulties. Combining data from boreholes with different orientations could enhance calibration constraints. The sensitivity to parameters controlling thermal stresses has not been explored, given the limited presence of DITFs in BS-1. Investigating the impact of thermo-elastic parameter heterogeneity on wellbore failure is essential.

It is important to note that the methodology relies on inverting principal stresses at the borehole wall, favoring the tangential stress as the maximum principal stress in BS-1. This may not hold universally, especially in scenarios with different internal well pressure and in-situ stresses, leading to unique breakout geometries that may challenge the methodology. Situations where breakouts initiate with large width ($> 90^{\circ}$) and result in total borehole collapse could also pose difficulties for the inversion approach.

The workflow and its scripts have been extensively enhanced (and is continuing to be improved as an on-going process) in order to be able to make it more versatile in terms of processing of input datasets and also the parameters that can be calibrated. In addition, the second order calibration simulator is capable of integrating additional point specific information/measurements (such as minifrac or SIMFIP measurements outputs) into the calibration to increase the robustness of the outputs. It is worthy of mentioning that as the on-going improvement, the workflow is being tested against larger diversity of data sets and in the meantime its efficiency and applicability in real case projects is improving.

7. CONCLUSIONS

In modern wellbore failure analyses, conventional methods often separate stress and strength estimations. Recognizing the limitations of such approaches, we introduce a novel methodology in this paper. This approach simultaneously assesses stress tensor components, orientations, and rock strength properties (cohesion, friction) within a robust probabilistic framework. Combining analytical and empirical solutions with the regularized pilot points method (implemented in PEST software), we utilize measurements like breakout width, extent, and orientation, along with the presence/absence of DITFs. Generic inclusion of estimated parameters, such as $Shmin$ interpreted from XLOT, is also feasible. Thermal stresses from borehole wall cooling are considered. Applied to the BS-1 borehole dataset in Basel

(Switzerland), our methodology enhances understanding of borehole failure processes, the interplay of failure parameters, and the variability of stress and strength conditions in the Earth's crust.

In utilizing a simplified stress computation around a cylindrical opening, we demonstrate that the Mohr–Coulomb criterion yields stress profiles consistent with independent observations. The consistently low stress gradients align with Valley and Evans' (2019) findings, suggesting potential non-uniform tectonic straining at the basement–cover interface. Moreover, the absence of breakouts in certain segments of BS-1 correlates with increased natural fracturing. Our parameter estimation approach indicates that the absence of failure involves a reduction in differential stress, moving towards isotropic conditions, likely due to stress relief and rock mass softening associated with fracturing, particularly near the basement–cover interface.

Our 2^{nd} order analyses suggest that both strength and stress heterogeneity contribute to borehole failure variability. We provide in-situ quantification of strength and stress parameters, with coefficients of variation (COV) around 13% for frictional parameters and 20% for cohesive strength parameters. Stress magnitude variations have a COV of about 10%. However, the variability in strength alone, assuming linear stress-depth relationships, is insufficient to explain the depth variability of DITFs and BOs orientation.

This workflow was initially developed by Dahrabou et al. (2022) for interpreting borehole failure information through analytical and empirical solutions for estimating wellbore stresses and failure parameters combined with the regularized pilot points method. We have advanced this method and applied it to different geothermal reservoirs such as BS-1 borehole in Basel geothermal project. The obtained logs (i.e. acoustic televiewer logs) were used and interpreted shortly after drilling of the boreholes to prepare datasets of borehole failures (i.e., breakout width, extent and orientation, and existence of DITFs).

These variable datasets are utilized to estimate model parameters. By applying our methodology, we are able to generate borehole profiles including, amongst others, the heterogeneous distributions (i) of the principal components of the stress tensor with corresponding directions, and (ii) of rock strength properties such as cohesion and friction as the major outcomes aiding us in reaching to our goal of being able to develop sustainable geothermal reservoirs by better understanding stress and strength variabilities. Meanwhile, this wellbore failure analysis approach establishes the foundation for quantitative wellbore failure prediction and risk analyses. These are essential for designing and deploying innovative borehole completions, crucial for unlocking the potential of deep EGS.

REFERENCES

Akaike H. A new look at the statistical model identification. IEEE Trans Autom Control 19 (6).

Alcolea A., Ramírez J., Medina A., Pilot points method incorporating prior information for solving the groundwater flow inverse problem, Advances in Water Resources, 29 (2006), pp. 1678-1689, 10.1016/j.advwatres.2005.12.009

Azzola J., Valley B., Schmittbuhl J., Genter A., Stress characterization and temporal evolution of borehole failure at the Rittershoffen geothermal project Solid Earth, 10 (4) (2019), pp. 1155-1180, 10.5194/se-10-1155-2019

Barton C., Zoback M., Burns K., In-situ stress orientation and magnitude at the Fenton geothermal site, New Mexico, determined from wellbore breakouts

Geophysical Research Letters, 15 (5) (1988), pp. 467-470

Borm G., Engeser B., Hoffers B., Kutter H., Lempp C., Borehole instabilities in the KTB main borehole. 1997. http://dx.doi.org/10.1029/96JB03669.

Brudy M., Zoback M. Compressive and tensile failure of boreholes arbitrarily-inclined to principal stress axes: Application to the KTB boreholes, Germany International Journal of Rock Mechanics and Mining Sciences, 30 (7) (1993), pp. 1035-1038, 10.1016/0148-9062(93)90068-O

Carrera J., Alcolea A., Medina A., Hidalgo J., Slooten L.J., Inverse problem in hydrogeology Hydrogeology Journal, 13 (2005), pp. 206-222, 10.1007/s10040-004-0404-7

Chang C., Zoback M.D., Khaksar A., Empirical relations between rock strength and physical properties in sedimentary rocks. Journal of Petroleum Science and Engineering. 2006;51(3):223–237. http://dx.doi.org/10.1016/j.petrol.2006.01.003.

Cuss R., Rutter E., Holloway R., Experimental observations of the mechanics of borehole failure in porous sandstone International Journal of Rock Mechanics and Mining Sciences, 40 (5) (2003), pp. 747-761, 10.1016/S1365-1609(03)00068-6

Dahrabou A., Valley B., Meier P., Brunner P., Alcolea A., A systematic methodology to calibrate wellbore failure models, estimate the in-situ stress tensor and evaluate wellbore cross-sectional geometry, International Journal of Rock Mechanics and Mining Sciences, Volume 149, 2022, 104935, ISSN 1365-1609, https://doi.org/10.1016/j.ijrmms.2021.104935.

Deichmann N., Giardini D., Earthquakes induced by the stimulation of an enhanced geothermal system below Basel (Switzerland) Seismological Research LettersSearch, 80 (5) (2009), pp. 784-798, 10.1785/gssrl.80.5.784

Doherty J., Ground water model calibration using pilot points and regularization Ground Water, 41 (2003), pp. 170-177, 10.1111/j.1745-6584.2003.tb02580.x

Häring M.O., Schanz U., Ladner F., Dyer B., Characterisation of the Basel 1 enhanced geothermal system. Geothermics. 2008;37(5):469–495. http://dx.doi.org/10.1016/j.geothermics.2008.06.002.

Kaeser B., Kalt A., Borel J. The crystalline basement drilled at the basel-1 geothermal site, a preliminary petrologicalgeochemical study (2007)

Kirsch G., Die theorie der elastizitat und die bedurfnisse der festigkeitslehre Z Ver Deutscher Ingenieure, 42 (1898), pp. 797-807

Lin W., Yamamoto K., Ito H., Masago H., Kawamura Y., Estimation of minimum principal stress from an extended leak-off test onboard the chikyu drilling vessel and suggestions for future test procedures. Scientific Drilling. 2008; 6:43–47. http://dx.doi.org/10.2204/iodp.sd.6.06.2008.

Mastin L., Heinemann B., Krammer A., Fuchs K., Zoback M., Stress orientation in the KTB pilot hole determined from wellbore breakouts. Scientific Drilling. 1991;2.

Medina A., Carrera J., Geostatistical inversion of coupled problems: dealing with computational burden and different types of data Journal of Hydrology, 281 (4) (2003), pp. 251-264

Schmitt D.R., Currie C.A., Zhang L., Crustal stress determination from boreholes and rock cores: Fundamental principles Tectonophysics (2012), pp. 1-26, 10.1016/j.tecto.2012.08.029

Shen B. Borehole breakouts and in situ stresses. In: First Southern Hemisphere International Rock Mechanics Symposium. 2008, p. 407–18.

Shen B., Stephansson O., Modification of the G-criterion for crack propagation subjected to compression Engineering Fracture Mechanics, 47 (2) (1994), pp. 177-189, 10.1016/0013-7944(94)90219-4

Setiawan N.B., Zimmerman R.W., A unified methodology for computing the stresses around an arbitrarily-shaped hole in isotropic or anisotropic materials International Journal of Solids and Structures, 199 (2020), pp. 131-143, 10.1016/j.ijsolstr.2020.03.022

Valley B., Evans K.F., Stress magnitudes in the Basel enhanced geothermal system. International Journal of Rock Mechanics and Mining Sciences. 2019;118(April):1–20. http://dx.doi.org/10.1016/j.ijrmms.2019.03.008.

Valley B., Evans K.F., Stress orientation to 5 km depth in the basement below Basel (Switzerland) from borehole failure analysis Swiss Journal of Geosciences, 102 (3) (2009), pp. 467-480, 10.1007/s00015-009-1335-z

Zang, A., & Stephansson, O., Stress field of the earth's crust. Springer Science and Business Media. (2010) https://doi.org/10.1007/978-1-4020-8444-7

Ziegler M., Valley B., Evans K.F., Fault orientations inferred from analysis of a microseismic cluster dataset of the basel EGS reservoir agree well with borehole fracture data Abstract Volume 13th Swiss Geoscience Meeting, Basel, 20th–21st November 2015: 7. Geothermal Energy, CO2 Sequestration and Shale gas, Swiss Academy of Sciences (2015), p. 219

Zoback M., Barton C., Brudy M., et al. Determination of stress orientation and magnitude in deep wells. Special issue of the ijrmms: rock stress estimation isrm suggested methods and associated supporting papers; International Journal of Rock Mechanics and Mining Sciences. Special issue of the ijrmms: rock stress estimation isrm suggested methods and associated supporting papers; 2003:1049–1076.http://dx.doi.org/10.1016/j.ijrmms.2003.07.001,

Zoback M.D., Reservoir Geomechanics. Cambridge University Press; 2007. http://dx.doi.org/10.1017/CBO9780511586477.